Journal of Directed Energy, **3**, Spring 2009, 118–133

Variation of the Dynamic Bidirectional Reflectance Distribution Function Across High-Energy Laser Spots

Larry McKee*

Directed Energy Test and Evaluation Capability Lead Systems Integrator, Science Applications International Corporation, 6200 Uptown Boulevard, NE, Suite 300, Albuquerque, New Mexico 87110

The capability to accurately measure the high-energy laser (HEL) irradiance incident on an airborne target is a key shortfall for HEL test and evaluation. The hope has been that analyzing remote imagery of the HEL spot on the target could provide the required measurement to an acceptable accuracy. The key feasibility issue for this technique is being able to identify and use an appropriate bidirectional reflectance distribution function (BRDF) for the target surface as the surface is being heated and damaged by the HEL interaction. However, experimental results and laboratory measurements show that the BRDF of a surface heated by a HEL is highly variable, both temporally and spatially. Further, no basis could be identified for predicting or determining the dynamic BRDF values across the laser spot without knowledge of the incident irradiance profile. Because the measurement objective is to determine the incident irradiance, the use of passive laser spot imagery alone is judged to be an impractical solution approach for range applications.

KEYWORDS: Bidirectional reflectance distribution function, Irradiance measurement, Remote imagery

Nomenclature

E_i	laser irradiance incident on target surface, W/cm^2
E_o	laser irradiance normal to the laser beam propagation direction, W/cm^2
f_r	bidirectional reflectance distribution function, 1/sr
L_r	radiance reflected from target surface, W/cm^2-sr
θ_i	polar angle of incidence for laser, deg
θ_r	polar angle of reflection, deg
ϕ_i	azimuthal angle of incidence for laser, deg
ϕ_r	azimuthal angle of reflection, deg

1. Introduction

During the Directed Energy Test and Evaluation Capability (DETEC) Tri-Service Study, the capability to accurately measure the high-energy laser (HEL) irradiance incident on an

Received September 29, 2008; revision received January 20, 2009.
*Corresponding author; e-mail: mckeel@saic.com.

airborne target was identified as a key shortfall for HEL test and evaluation. The hope was that analysis of remote imagery of the HEL spot on the target could provide the required measurement to an acceptable accuracy. For this reason, the requirement to measure HEL irradiance on target was combined with the requirement for multispectral target imagery in the HEL Airborne Target Irradiance and Imagery Measurement (ATIM) capability to be addressed by DETEC.

However, the HEL ATIM analysis of alternatives determined that the ability to accurately measure HEL irradiance on target from analysis of remote imagery was a high-risk approach. This technique relies on scatter of the laser off of the target, and the main issue was risk in being able to identify and use an appropriate bidirectional reflectance distribution function (BRDF) for the target surface as the surface was being heated and damaged by the HEL interaction. Although the BRDF of a material can be measured in the laboratory under benign conditions (i.e., when the material is not being heated by a laser), results from Bailey et al.[1] and from McKee[3] showed that the BRDF could be expected to change during HEL irradiation. Measurements of time-varying, or dynamic, BRDF require the simultaneous sampling of a range of reflection angles (rather than sequential sampling of each angle), and the scatter screen technique was developed to accomplish this for a range of reflection angles.[1]

However, the scatter screen data give only "spot-averaged" BRDF values (because the irradiance incident on each point of the scatter screen is due to reflections from the entire laser spot) and do not provide information on potential variations of BRDF across the laser spot. Because spatially resolved BRDF values across the spot are needed to determine laser-irradiance-on-target maps from remote spot imagery, it was necessary to perform experiments specifically designed to measure spatially resolved target BRDF under HEL heating conditions. Results of such experiments and their implications for HEL ATIM are presented here.

2. BRDF Determination from Target Reflections

Consider a collimated laser beam with irradiance distribution $E_i(x, y)$ incident on a flat target at angles θ_i, ϕ_i, where x, y are coordinates in the flat target plane measured from the laser spot center. The angle θ_i is measured from the target normal (z axis), and ϕ_i is measured in the x–y (target) plane relative to the $+x$ direction (Fig. 1). Then the radiance reflected by the target at point x, y into the angle θ_r, ϕ_r is given by

$$L_r(x, y, \theta_r, \phi_r) = f_r(\theta_i, \phi_i, \theta_r, \phi_r, x, y)\, E_i(x, y), \tag{1}$$

where $f_r(\theta_i, \phi_i, \theta_r, \phi_r, x, y)$ is the target BRDF for a laser beam incident at angles θ_i, ϕ_i and at point x, y and for scattering into angles θ_r, ϕ_r and where θ_r is the polar angle measured from the target normal (z axis) and ϕ_r is the azimuthal angle measured in the x–y (target) plane relative to the $+x$ direction (Fig. 1). The functional form of the BRDF in Eq. (1) allows for variation within the laser spot on the target. Note that the irradiance incident on the target surface E_i is related to the irradiance normal to the laser beam propagation direction E_o by $E_i = E_o \cos(\theta_i)$ at each point in the laser spot.

If the BRDF is known, Eq. (1) can be used to determine the incident irradiance from measurements of the reflected radiance:

$$E_i(x, y) = L_r(x, y, \theta_r, \phi_r)/f_r(\theta_i, \phi_i, \theta_r, \phi_r, x, y). \tag{2}$$

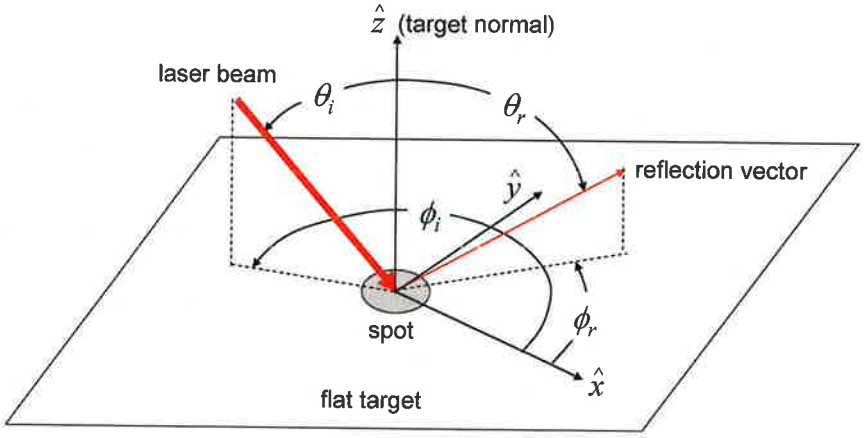

Fig. 1. Laser–target reflection geometry.

Conversely, if the incident irradiance is known, Eq. (1) can be used to determine the BRDF from measurements of the reflected radiance:

$$f_r(\theta_i, \phi_i, \theta_r, \phi_r, x, y) = L_r(x, y, \theta_r, \phi_r)/E_i(x, y). \tag{3}$$

When Eq. (3) is applied in the scatter screen technique, a camera images the screen and each camera pixel measures the radiance reflected by the entire laser spot at the corresponding reflection angle. The resulting "spot-averaged" BRDF can be used to relate total radiance reflected at each angle to the total laser power incident on the target and can be applied to hazard predictions.[1]

To determine BRDF values across a laser spot, a camera directly images the spot and Eq. (3) is applied to each camera pixel. In this case, only reflectance values at a single pair of incidence and reflection angles can be determined and not the BRDF. In other words, by imaging the laser spot directly rather than secondary reflections from a scatter screen, spatial resolution of reflectance across the spot is obtained at the expense of angular distribution information. This direct imagery technique is used here to determine whether and how reflectance varies across a HEL spot as a result of target heating and damage.

3. Experimental Setup

A test series to investigate dynamic BRDF was conducted in January 2008 at the Optical Radiation Branch of the Air Force Research Laboratory (AFRL/RHDO) using their 3-kW IPG Photonics ytterbium fiber laser (wavelength 1.07 μm) to heat 16-gauge (0.0625-in.-thick) 2205 duplex stainless steel (DSS) painted with 383 olive green chemical agent–resistant coating (CARC). Figure 2 shows the basic experiment layout. The laser was incident on the target at near-normal incidence ($\sim$1 deg), and dynamic reflectance values were calculated from imagery data collected at a 45-deg reflection angle in the plane of incidence ($\theta_i \cong 1$ deg, $\theta_r = 45$ deg, $\phi_i = \phi_r = 0$ deg). Radiance for each image pixel was divided by the incident irradiance corresponding to that pixel to generate a reflectance map for each camera frame (frame rate 60 Hz). In addition, scatter screen BRDF data were collected simultaneously by locating the screen on the opposite side of the target normal (Fig. 2). InGaAs cameras with narrowband-pass filters were used to collect target reflection

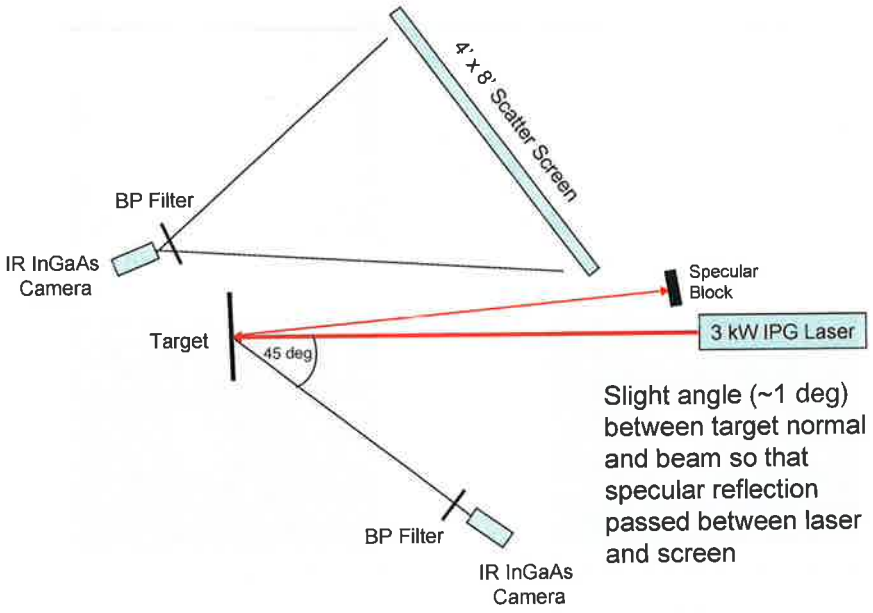

Fig. 2. Experiment layout for dynamic BRDF test series.

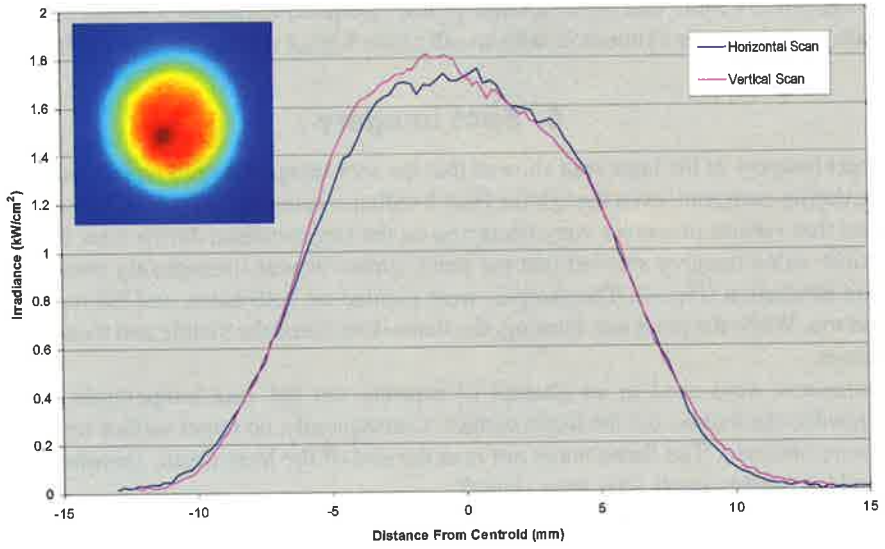

Fig. 3. Laser spot image (on uniform diffuse target) and irradiance profile scans.

and scatter screen imagery at the laser wavelength while minimizing detection of target hot spot thermal emissions. Additional diagnostics included pyrometers for determining surface temperatures.

The laser output power was varied to illuminate the 2 × 2 in. coupon targets at 2,500, 1,300, and 640 W over a 17-mm-diameter spot ($1/e^2$ diameter). The irradiance at the centroid for the various powers was about 1.72, 0.88, and 0.44 kW/cm^2, respectively. The spot irradiance profile is shown in Fig. 3; the same spot size and profile shape applied for

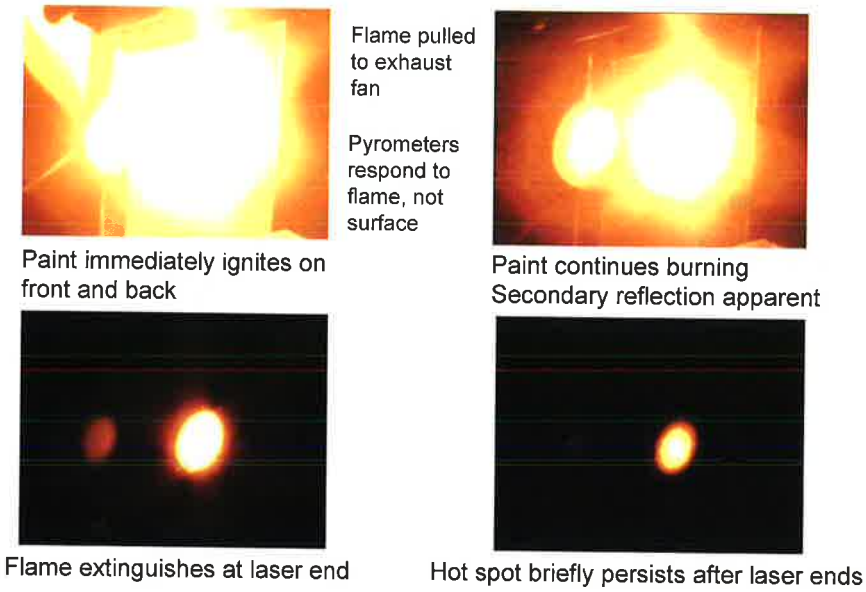

Fig. 4. Video frames of target for full-power shot.

the lower powers. Note that the irradiance profile (assumed to remain constant throughout all shots) was basically symmetric with an off-center higher irradiance region ("hot spot").

4. Spot Imagery

Direct imagery of the laser spot showed that the spot image changed rapidly and significantly during each shot, even though the laser irradiance remained constant. These changes implied that various processes were occurring on the target surface during laser heating.

Visible video imagery showed that the paint ignited almost immediately after the start of laser irradiation (Fig. 4). The samples were painted on both sides, and the rear surface ignited too. While the paint was burning, the flame dominated the visible and thermal target emissions.

Pyrometers were used in an attempt to measure the hot spot temperature, but they responded to the flames, not the target surface. Consequently, no target surface temperature data were obtained. The flame burns out near the end of the laser dwell, revealing the hot spot, which quickly cools after laser shutoff.

Posttest photos of the target samples for the three laser powers give better indications of the various target responses during laser irradiation (Fig. 5). As the paint burned, a carbon residue (char) layer formed, and the laser began eroding/removing the char. At full power, the underlying metal was exposed near the end of the dwell and began melting. Note that the full-power sample in Fig. 5 displays all of the various response processes at different radial distances; increasing radial distance corresponds to decreasing fluence, so that metal exposure and melting requires the most fluence and paint pigment decomposition the least.

It is interesting to note that all three shots correspond to the same fluence. Hence, the degree of damage and surface change depended on both fluence and irradiance. Also, Fig. 5 shows that smoke and debris from the burning paint were pulled to the left by an exhaust fan and deposited on that side of the damage spot. This figure also shows that the smoke/debris

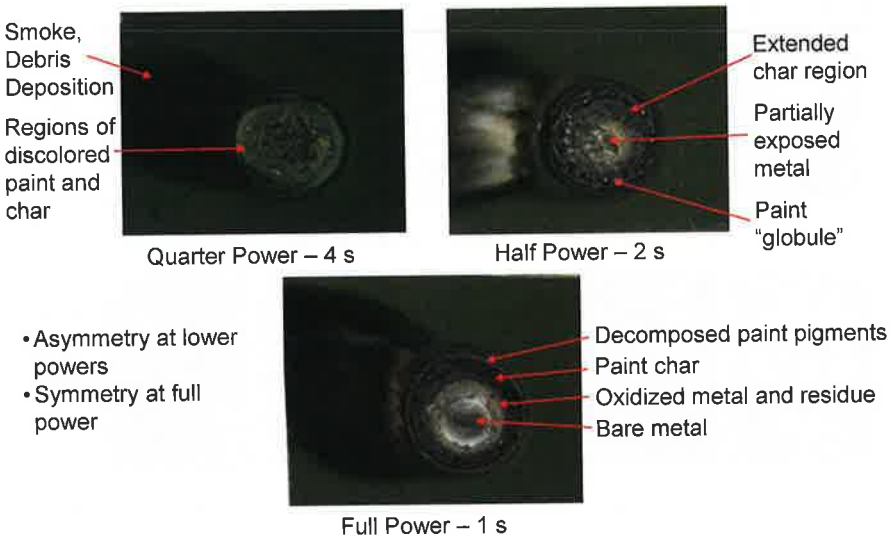

Fig. 5. Posttest photographs of target samples for various HEL powers.

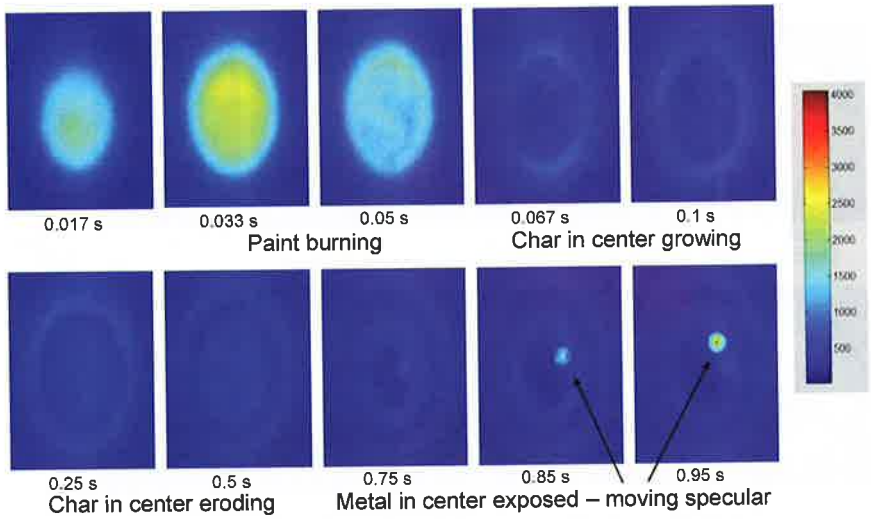

Fig. 6. Spot image at 45 deg for full-power shot CRP032 (irradiance at centroid = 1.7 kW/cm^2). Units for color scale are pixel counts.

deposition area displayed different colors, depending on the laser power (another indication of different processes in action at each power/irradiance).

Examples of direct imagery of the laser spot (after noise/background subtraction†) are shown in Figs. 6–8 for the three laser powers. These figures indicate changes in spot imagery due to the paint burning and charring, the char region growing and eroding, and

†Typical average noise/background was 225 counts, so that corrected counts below 15 are not valid. Corrected counts of 100 or higher have uncertainties of less than ±15%.

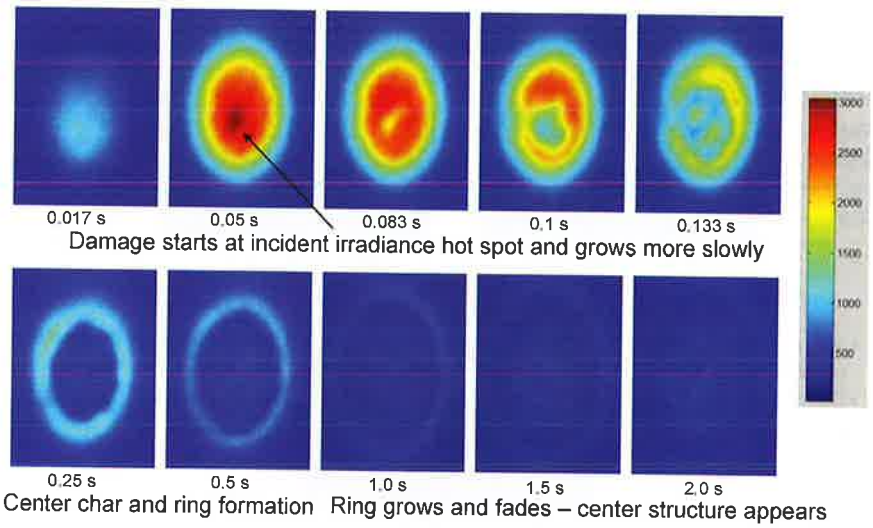

Fig. 7. Spot image at 45 deg for half-power shot CRP042 (irradiance at centroid = 0.9 kW/cm^2). Units for color scale are pixel counts.

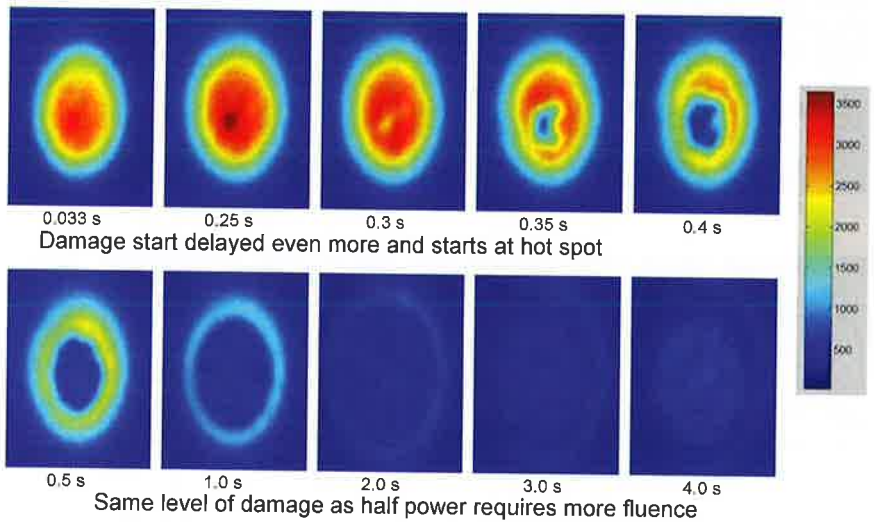

Fig. 8. Spot image at 45 deg for quarter-power shot CRP053 (irradiance at centroid = 0.4 kW/cm^2). Units for color scale are pixel counts.

the underlying metal being exposed and melting for the full-power shots (Fig. 6). As the metal surface melted and deformed at full power, specular reflections were seen to occasionally move through the camera field of view (Fig. 6).

For the full-power shots, the spot image intensity quickly decreased (Fig. 6); no camera frames displayed the incident spot profile. The largest drop in intensity was at the spot center, where char rapidly formed and grew in radial extent.

Initial frames of the half- and quarter-power shots did display the incident spot profile (Figs. 7 and 8). Paint damage was slower for these powers, and the early frames show the

paint uniformly scattering the incident irradiance. Note that the evidence of BRDF change begins at the hot spot and grows from that point until a ring appears. The ring (which encircles the char region) eventually fades, and there is little scatter from the target near the end of the laser dwell.

The spot images imply that the target reflectance quickly changes and that the changes are not uniform over the laser spot. The nonuniform reflectance causes the spot scatter to lose the features of the incident irradiance profile. This "distortion" in the scatter would need to be corrected by application of the correct dynamic BRDF value to each frame and pixel in order to retrieve the incident irradiance profile.

Also, the scatter from this type of target quickly decreases due to the paint charring. When the underlying metal is exposed, the target scatter is even lower. This will result in low signal-to-noise values for long-range outdoor testing and makes it very difficult to recover spot features near the center.

5. Dynamic Target Reflectance

The intention for this experimental series had been to convert the spot imagery into dynamic reflectance maps by dividing the reflected radiance measured for each pixel by the incident laser irradiance for that pixel. Unfortunately several complications were encountered in implementing this approach, as detailed below.

There was a problem in calibrating the camera pixel counts to determine radiance. The calibration approach attempted was to use a target with known static and uniform BRDF and image a low-power laser spot on that target. (The laser power on target was reduced to 110 W so that insignificant surface heating would result and the static BRDF value would be appropriate.) However, the initial (i.e., predamage) dynamic reflectance values obtained with this calibration were significantly higher than the static value of painted DSS measured pretest. Because the cause of the discrepancy could not be identified, the reflectance values determined from spot imagery must be regarded as relative values.

There was a problem in registering the spot image to the incident laser profile for the reflectance calculation. Target samples were manually mounted on a holder for each shot, and post test it was discovered that the beam position in the camera images was not consistent between tests, varying by as much as 2 mm. To correct for this, the spot imagery for each shot was recentered based on the center of the first image where the laser was fully on. Errors from image misalignment were lowest near the centroid of the incident laser profile, as the profile was relatively flat there.

The incident laser profile image exhibited significant pixel-to-pixel variations, likely due to speckle in the scatter plate image. Two correction techniques were used. First, instead of using the scatter plate image, the initial frames of the quarter-power shots were analyzed. The CARC paint is a good Lambertian scattering surface before it is damaged. The initial frames of six quarter-power shots were aligned and averaged pixel by pixel. The incident laser profile line scans in Fig. 3 are the results. Second, for analysis of reflections at the spot centroid, the reflected signal was averaged over a 2-mm square (11 $\times$ 11 pixels) centered on the initial spot.

Examples of relative reflectance maps for the three powers shot are given in Figs. 9–11.[‡] As with the spot images, significant spatial and temporal variations in reflectance values are

[‡]The relative reflectance values in these maps and in subsequent figures have estimated accuracies of $\pm 25\%$, including errors due to hot spot thermal emission leakage through the camera band-pass filter.

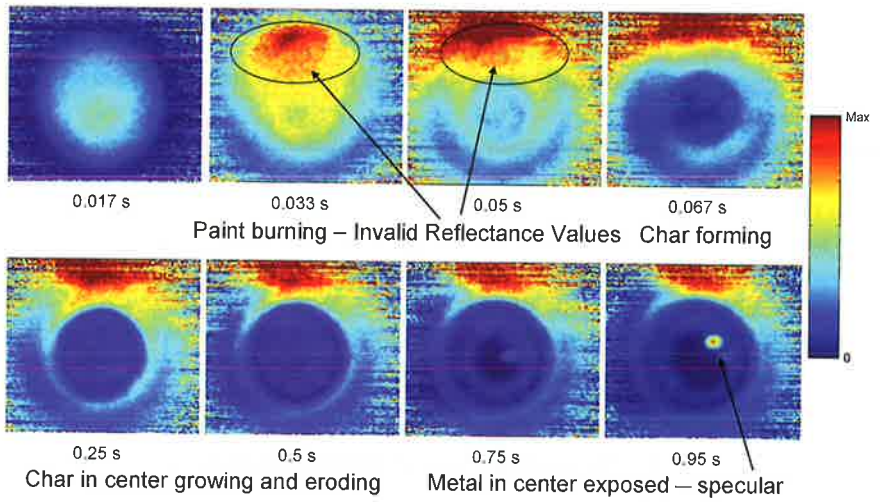

Fig. 9. Relative reflectance maps ($\theta_r = 45$ deg) for full-power shot CRP032 (irradiance at centroid = 1.7 kW/cm^2).

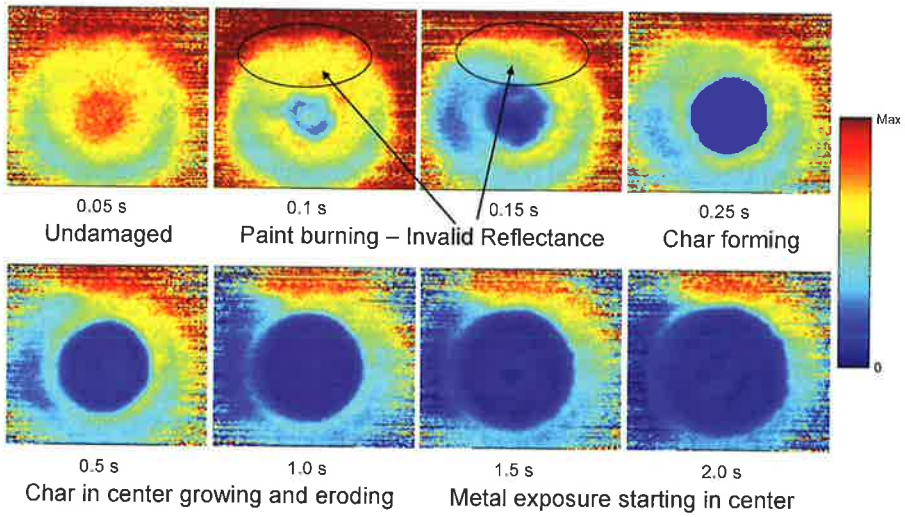

Fig. 10. Relative reflectance maps ($\theta_r = 45$ deg) for half-power shot CRP042 (irradiance at centroid = 0.9 kW/cm^2).

evident due to paint burning, charring, char removal, metal exposure, and metal melting. In these reflectance maps, values outside of the laser spot are not valid; values in this region are dominated by imagery noise after average background subtraction and are especially susceptible to the problems noted above.

Note that the flame from the burning paint can invalidate the reflectance calculation, as can smoke and debris from the burning paint. During the testing, an exhaust fan pulled the smoke and debris to the left so that the left-hand side of the reflectance maps may also have questionable values when the paint is burning.

Figures 9–11 verify the implications from the direct spot imagery concerning dynamic BRDF behavior. Initially, a region of low reflectance forms and grows as the paint

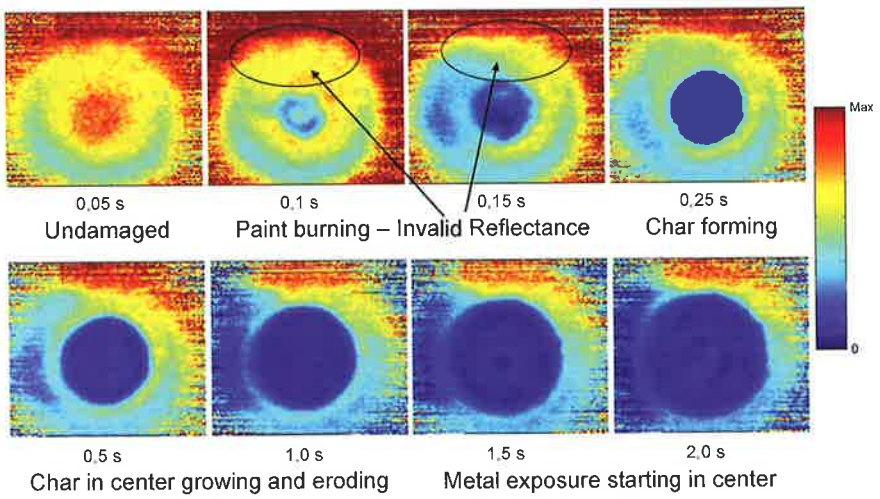

Fig. 11. Relative reflectance map ($\theta_r = 45$ deg) for quarter-power shot CRP053 (irradiance at centroid = 0.4 kW/cm^2).

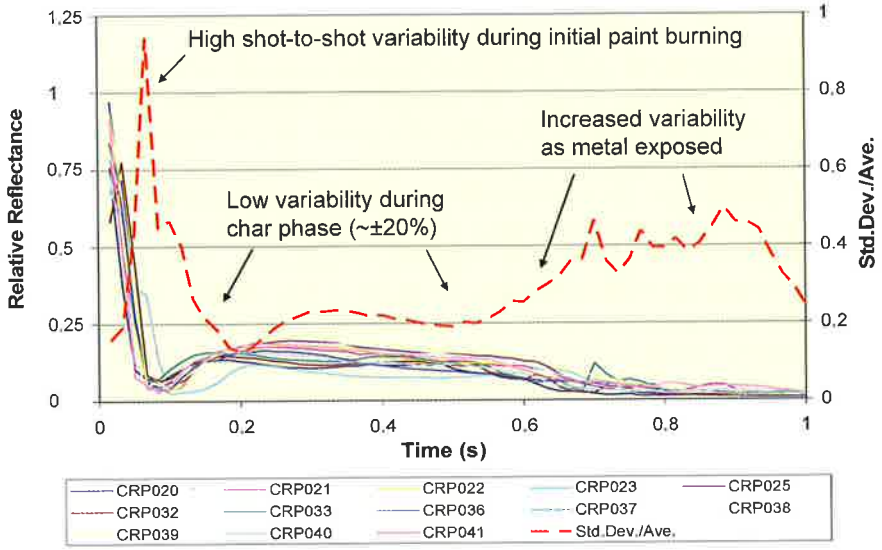

Fig. 12. Reflectance values ($\theta_r = 45$ deg) at spot centroid versus time for various full-power shots. Shot-to-shot variability (standard deviation/average) versus time is also plotted.

chars and the char extent expands. This char region appears to have relatively uniform (but low) reflectance. Later, the reflectance decreases further as the underlying metal is exposed.

Repeatability of the dynamic reflectance behavior was investigated by examining a number of full-power shots. Figure 12 shows the relative reflectance value at the laser spot centroid versus time (from the 2-mm square average). Note that the degree of variability of the reflectance values depends on the phenomena occurring at the different times.

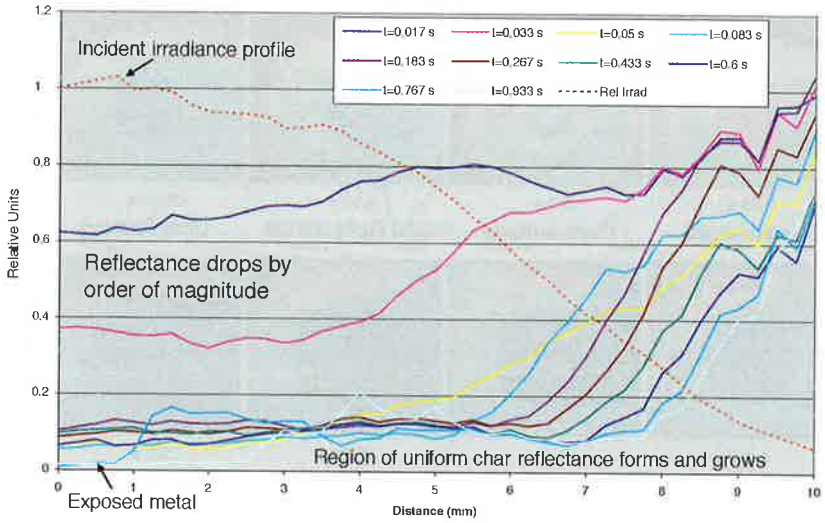

Fig. 13. Relative reflectance values ($\theta_r = 45$ deg) versus distance from spot center at various times for full-power shot CRP032.

Shot-to-shot centroid reflectance variability was also analyzed for the lower power shots and found to be somewhat smaller. For example, the quarter-power shots exhibited a variability of $\pm 12\%$ during their extended char phase, as compared to $\pm 25\%$ for the full-power shots during this phase.

To better quantify how the relative reflectance values change spatially and temporally across the spot, reflectance values along a horizontal line from the spot center to the spot edge (this avoids the anomalous region containing burning paint, smoke, and debris) were determined. Results for a full-power shot are shown in Fig. 13. Note that the reflectance varies by up to an order of magnitude, both spatially and temporally.

The reflectance spatial variations can be related to the incident irradiance profile in Fig. 13; regions of high irradiance have the largest changes, and vice versa. However, the reflectance changes are not simply related to accumulated fluence. For example, the relative reflectance values initially change rapidly as the paint is burned at the spot center but remain nearly constant as the resulting char is slowly removed (even though fluence continues to accumulate there at a constant rate).

The relative reflectance data for Fig. 13 are replotted versus time for various distances in Fig. 14. Relative BRDF data obtained using the AFRL/RHDO scatter screen technique for the same shot are also plotted for comparison. Figure 14 shows that the reflectance temporal behavior across the spot strongly depends on location (because incident irradiance varies with location in the spot). Also notice that the various spatial values are significantly different from the scatter screen (spot-averaged) value. The scatter screen temporal behavior is generally smoother than the spatial values and implies significant contributions from the spot edge.

Results for the two lower laser powers showed similar spatial and temporal changes, but on longer time scales. This is illustrated in Fig. 15, which shows relative reflectance values at the spot center versus time for the three laser powers. Because the spot size was the same for all three powers, the centroid irradiance was proportional to the total power, with

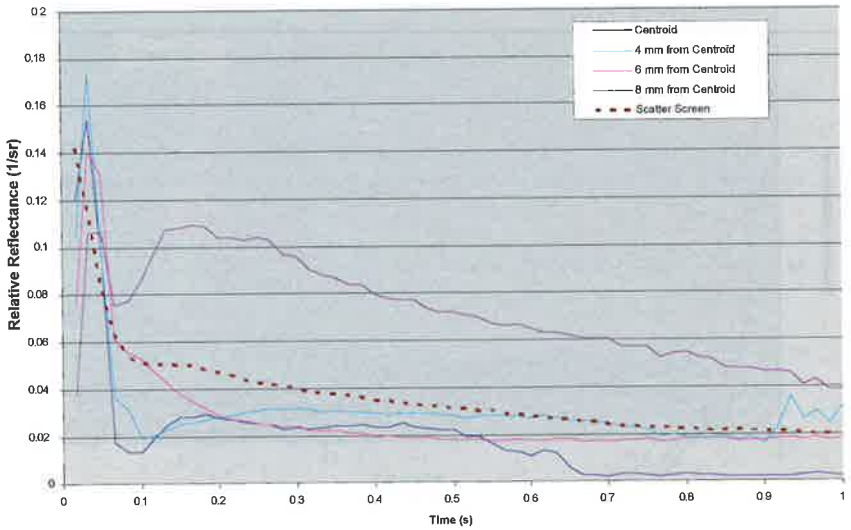

Fig. 14. Relative reflectance values ($\theta_r = 45$ deg) versus time at various distances from spot center for full-power shot CRP032. Scatter screen data ($\theta_r = 45$ deg, $\phi_r = 0$ deg) for the same shot are plotted for comparison.

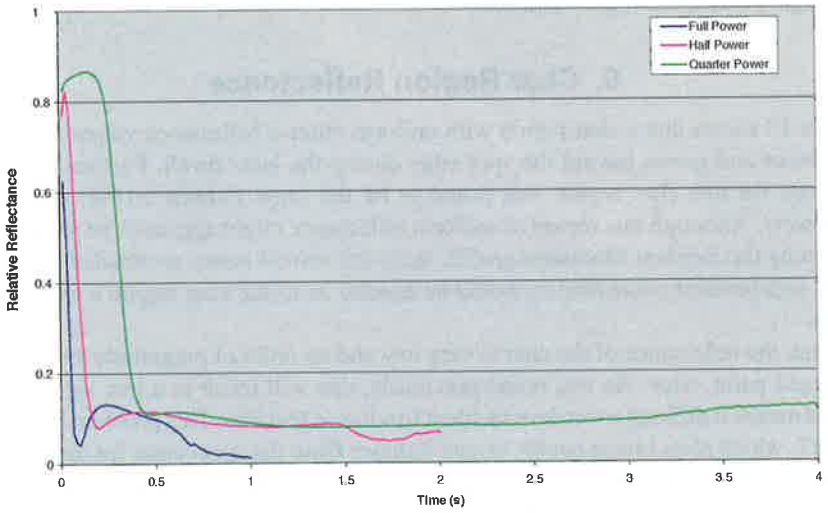

Fig. 15. Average relative reflectance values ($\theta_r = 45$ deg) at spot centroid versus time for various laser powers. (Values have been averaged over all shots of a particular power.)

values of 1.72, 0.88, and 0.44 kW/cm^2. Although there are similar changes in reflectance values for the three irradiances, the highest irradiance case shows more variation than the other two. (This is consistent with the posttest sample photographs, which showed that full-power shots exhibited the most different "response regions.")

When the data in Fig. 15 are plotted versus energy on target, rather than time, it becomes clear that dynamic relative reflectance depends on both fluence and irradiance (Fig. 16), as

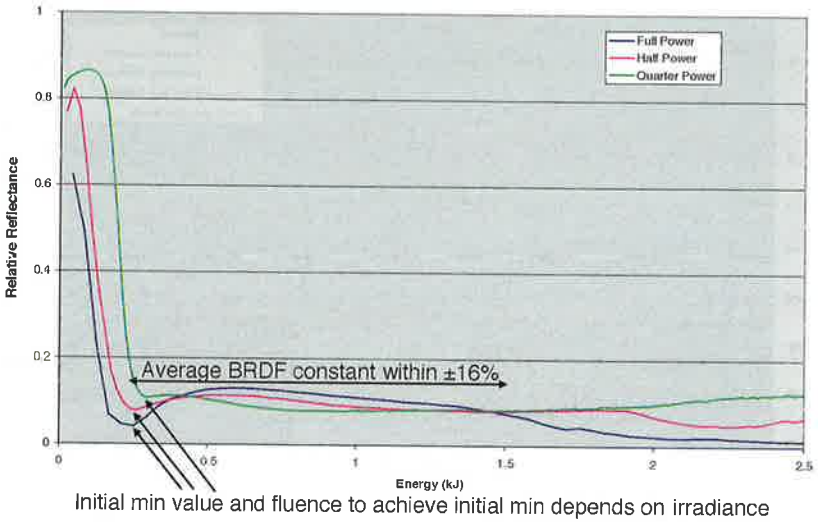

Fig. 16. Average relative reflectance values ($\theta_r = 45$ deg) at spot centroid versus energy on target for various laser powers.

was indicated by the posttest sample photographs (Fig. 5), previous test results,[3] and the spot imagery (compare Figs. 7 and 8).

6. Char Region Reflectance

Figure 13 shows that a char region with uniform relative reflectance values forms at the beam center and grows toward the spot edge during the laser dwell. Further, the relative reflectance for this char region was found to be the same (within ±16%) for all three laser powers. Although this region of uniform reflectance might appear to be promising for determining the incident irradiance profile, there are several issues as detailed below.

First, independent confirmation would be needed as to the char region's existence and location.

Second, the reflectance of the char is very low and an order of magnitude lower than the undamaged paint value. As was noted previously, this will result in a low signal-to-noise ratio and makes it difficult to retrieve incident irradiance features. This problem is illustrated in Fig. 17, which plots image counts versus distance from the spot center for three different laser powers.[§] The times selected correspond to those during which char exists over most of the spot and also to equivalent fluences for the different powers. Features of the incident irradiance profile are lost in the low-reflectance char region, and the transition to the higher reflectance region outside the char area is not obvious.

Finally, HEL testing of painted metal targets in high-speed airflow conditions has shown that black paint char never really forms.[2] Testing of DSS samples with green paint (not CARC) showed that with no air flow, a black char layer quickly formed, followed by subsequent removal/erosion of the char starting in the laser spot center and moving to the

[§]Camera frame integration time and f-stop were adjusted for each laser power to give about the same maximum number of counts for the brightest frame/pixel, resulting in about the same number of counts in the char region.

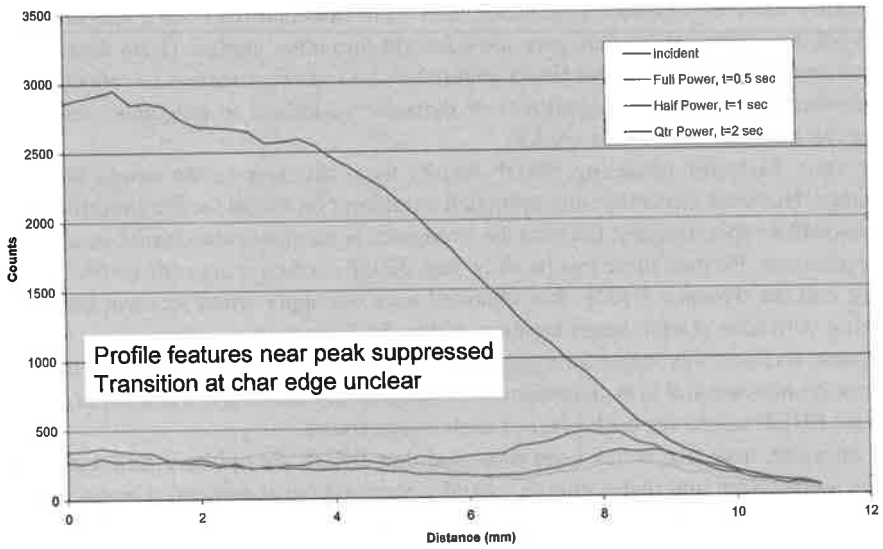

Fig. 17. Laser spot image counts versus distance from spot center for various laser powers. Selected times correspond to large char region extents.

edges. This behavior is completely consistent with the current test series. However, with Mach 0.7 airflow, the paint burned into a light tan residue almost immediately, followed by subsequent exposure and darkening of the underlying steel substrate. During the high-speed airflow testing, there was no flame and no smoke/soot/debris deposition on the target. Hence, the existence of the char region cannot be relied on for high-speed missile targets.

7. Experimental Series Conclusions

Results from this experimental series support the following conclusions.

The technique of computing spatially resolved BRDF values from laser spot imagery proved to be difficult to implement. Problems with radiometric calibration, imagery alignment, and incident laser spot profiling prevented absolute determination of reflectance values. Future attempts to measure dynamic BRDF for a laser-heated material should consider either improvements to this technique or a different approach.

Reflectance values of the painted metal target were found to be highly dynamic, both temporally and spatially. The reflectance values varied by up to an order of magnitude across the HEL spot.[¶] Static uniform BRDF values cannot be used.

Reflectance values across the spot varied significantly from the spot-averaged value throughout the laser dwell. The spot-averaged values from scatter screen data do not represent local reflectance values and could not be used to accurately determine incident irradiance from spot imagery.

[¶]The relatively low shot-to-shot variability observed in the relative reflectance data (e.g., Fig. 12) was only for time-correlated data and a fixed laser power and applies only to repeatability of the experimental setup used; this variability does not give the uncertainty/error in modeling or predicting reflectance values for different setups, conditions, or scenarios (especially outdoor flight testing) or determining reflectance by another method.

Spatially resolved dynamic reflectance data were obtained only for a single reflection angle, but the scatter screen data give some insight into other angles. These data show that the spot-averaged BRDF for this target material is not a strong function of reflection angle. The implication is that the magnitudes of dynamic variations in reflectance observed at 45 deg can be expected at other angles.

The only basis for modeling BRDF results from this test series would be incident irradiance. However, this modeling approach would not be useful for determining incident irradiance from spot imagery, because the irradiance is unknown and cannot be assumed in this application. Further, these results show that BRDF evolution depends on the irradiance history, and the dynamic BRDF data obtained may not apply when incident irradiance is changing with time at each target location within the laser spot.

Because no basis was found for a predictive dynamic BRDF model when the incident irradiance is unknown and to be determined, an independent technique is needed to determine dynamic BRDF values for each pixel of each image frame.

As an aside, note that it has been proposed that BRDF should be a function of target surface temperature and that a remote spatially resolved measurement of temperature can be used to determine BRDF values across the laser spot. There are issues with this approach. First, a unique relationship between BRDF and temperature has yet to be established for a laser-heated target. Heating rate and surface state (e.g., char, oxidized metal, bare metal) appear to be major factors too. Second, the accuracy of determining spatial temperature maps from passive thermal imagery has not been quantified for laser-heated targets. Knowledge of target emissivity is needed to compute temperature from thermal radiance, and emissivity, like BRDF, is expected to vary with surface temperature, heating rate, and surface state. Hence, an independent technique would be needed to determine dynamic emissivity for each pixel of each image frame. This approach seems to be susceptible to numerous potential errors. Errors in determining emissivity would propagate into errors in determining surface temperature, which propagate into errors in determining reflectance values, which propagate into errors in determining incident irradiance.

8. Implications for HEL ATIM

The HEL ATIM objective is to determine the HEL irradiance incident on a flight target using remote imagery. Because no basis could be identified for predicting or determining the dynamic BRDF values across the laser spot without knowledge of the incident irradiance profile, this implies that the use of passive laser spot imagery alone as a solution will be very difficult. The results here are for laboratory testing of stationary targets, an ideal situation. Range testing of flight targets would present further complications with dynamic angles of incidence and reflection and degraded imagery. Thus, range applications become even more impractical.

Although irradiance on target may not be determined to an adequate accuracy, remote imagery of the laser spot still might be useful for estimating spot size and location on the target. However, there are complications in doing even this. As Figs. 6–8 show for the painted samples, only the initial camera frames have spot images that represent the incident irradiance profiles and allow the incident profile diameters to be determined. After these initial frames, the BRDF values rapidly change nonuniformly across the spot, resulting in distortions of the spot image relative to the incident profile. At later times, there is almost no scatter from the incident irradiance peak, and only a ring at the spot edge is evident. The diameter of the ring grows and only gives an estimate of the $1/e^2$ spot diameter. At

even later times, there is almost no scatter from the target for estimating spot size or location.

Concerning spot centroid location, the images maintained a degree of symmetry (due to reflectance symmetry), which seems to support this. However, if the spot moves (or the target rotates) during the laser dwell, this symmetry could no longer be relied on. Target material entering the spot on one side will have less accumulated damage than material exiting the spot on the opposite side, resulting in an asymmetric reflectance relative to the spot centroid.

Because HEL spot imagery can give useful information on the laser–target interaction, the DETEC program will continue to develop remote multispectral imagery capabilities for range testing applications. However, analysis of remote passive in-band imagery to determine HEL irradiance on target is no longer viewed as a practical approach. Instead, techniques for directly measuring irradiance on flight targets will be investigated through the Directed Energy Test Science and Technology program.

References

[1]Bailey, A., E. Early, K. Keppler, V. Villavicencio, P. Kennedy, R. Thomas, J. Zohner, and G. Megaloudis, J. Laser Applic. **20**(1), 22 (2008).

[2]Jungk, J., "Airflow Effects on High Energy Laser Irradiation of Painted Targets," 2008 Directed Energy Systems Symposium, High Energy Laser Lethality Conference 2008, Monterey, CA, March 3–7, 2008.

[3]McKee, L., "Bi-directional Reflectance Distribution Function Results from Outdoor HEL Testing," 2008 Directed Energy Systems Symposium, High Energy Laser Lethality Conference 2008, Monterey, CA, March 3–7, 2008.

The Author

Dr. Larry McKee received his Ph.D. in physics from the Naval Postgraduate School in 1972. He joined Science Applications International Corporation in 1989 after 20 years as an Air Force officer. His laser-related experience includes laser effects experimentation and modeling, high-energy-laser short course development and instruction, and high-energy-laser test and evaluation requirements development and related testing capability shortfall analysis. He is currently the Chief Scientist for the Directed Energy Test and Evaluation Capability Lead Systems Integrator and is responsible for technical direction of upgrades to the national test ranges' high-energy-laser testing capability.